Climatic Change (2024) 177:94
https://doi.org/10.1007/s10584-024-03752-z

Mesoscale convective system activity in the United States under intermediate and extreme climate change scenarios

Alex M. Haberlie[1] · **Brendan Wallace**[1,2] · **Walker S. Ashley**[1] · **Vittorio A. Gensini**[1] · **Allison C. Michaelis**[1]

Received: 31 October 2023 / Accepted: 21 May 2024

Abstract
The importance of mesoscale convective systems (MCSs) and their precipitation is well-established, and any future spatiotemporal shifts in their frequency or intensity could have far-reaching societal impacts. This work describes how MCS activity in the conterminous United States east of the continental divide (ECONUS) is modified by two future climate change scenarios. For this study, MCSs are identified in output from a convection-permitting regional climate model (CP-RCM) for three 15-year periods—namely, a retrospective baseline (1990–2005) and two end-of-century (2085–2100) climate change scenarios based on RCP 4.5 (EoC 4.5) and RCP 8.5 (EoC 8.5). The data reveal an eastward shift in regional MCS activity. Annually, days with MCSs largely remain the same or decrease west of the Mississippi River, whereas areas east of the Mississippi River experience more MCS days and MCS precipitation. The largest seasonal increases in MCS days and precipitation occur during the spring in parts of the Midwest and Northeast, whereas the largest decreases occur in parts of the Southern Plains during the summer. Overall, EoC 8.5 produced larger regional changes compared to EoC 4.5, suggesting that future CP-RCM experiments could benefit from considering multiple climate change scenarios.

Keywords Mesoscale systems · Thunderstorms · Precipitation · Regional models · Climate change · Thunderstorms · Climatology

1 Introduction

Mesoscale convective systems (**MCSs**) are a substantial precipitation producer in tropical, subtropical, and midlatitude climates across the world (Nesbitt et al. 2006; Houze 2018; Schumacher and Rasmussen 2020; Feng et al. 2021). For many locations in the eastern two-thirds of the conterminous United States (ECONUS), MCS precipitation accounts for the majority of warm-season precipitation (Schumacher and Rasmussen 2020). MCSs are

✉ Alex M. Haberlie
ahaberlie1@niu.edu

[1] Department of Earth, Atmosphere, and Environment, Northern Illinois University, DeKalb, IL, USA

[2] Argonne National Laboratory, Lemont, IL, USA

comprised of many deep, moist convective updrafts that interact through various meso-gamma to meso-beta (~ 10–100 km) processes and can last for several hours (Markowski and Richardson 2011; Houze 2018). These events maintain water and energy budgets, impacting weather-sensitive industries (e.g., agriculture, shipping, transportation) and infrastructure (e.g., river control structures, roads, power delivery and generation; Schumacher and Rasmussen 2020). Additionally, MCSs can produce severe weather that can have further deleterious effects on society (Ashley et al. 2019). In summary, MCSs are an important aspect of regional climates, and potential changes in their spatiotemporal character and precipitation may have widespread societal impacts. Due to their importance and potential sensitivity to climate change (Schumacher and Rasmussen 2020), the purpose of this work is to quantify end-of-century MCS activity in a new suite of high-resolution regional climate simulations (Gensini et al. 2023). Specifically, this work addresses two related research questions:

1) Do intermediate and/or pessimistic climate change scenarios result in a significant change in the frequency of days with MCS events in the ECONUS?
2) Do intermediate and/or pessimistic climate change scenarios result in a significant change in the amount of precipitation produced by MCS events in the ECONUS?

Environments supportive of MCS development and maintenance are projected to increase in frequency and coverage during the 21st century over the CONUS (Feng et al. 2016; Schumacher and Rasmussen 2020 and references therein). Clausius-Clapeyron scaling (Trenberth et al. 2003) provides a theoretical foundation that supports this trend—namely, increases in atmospheric moisture content, precipitation rates, and instability are driven by increases in temperatures in the lower troposphere and ocean (Brooks 2013; Diffenbaugh et al. 2013). Conversely, there is less confidence in the impact of convective inhibition on MCS environments in future climates (Schumacher and Rasmussen 2020). Studies that have examined convective inhibition in reanalysis data (Riemann-Campe et al. 2009; Taszarek et al. 2021; Andrews et al. 2024) and general circulation model (GCM) data (Lepore et al. 2021) suggest an increasing strength and/or frequency of capping inversions over parts of the CONUS, which could suppress thunderstorm activity. However, an explicit examination of how these trends influence MCSs activity is limited by the horizontal grid spacings (~ 10 to ~ 100 km) employed by these works (Kendon et al. 2021). This is because explicit simulations of crucial meso-gamma processes related to MCS sustenance (e.g., cold pool development; Squitieri and Gallus 2022a, b; Prein et al. 2021) require grid spacings of less than 4 km (Weisman et al. 1997).

The usage of convection-permitting regional climate models (CP-RCMs) further refines our understanding of regional climate change by explicitly simulating the combined effects of changes in environments *and* processes at various spatial scales. Deep, moist convection is an example of an atmospheric phenomenon that requires the juxtaposition of favorable large- and small-scale conditions (Doswell 1987; Doswell et al. 1996) and is important to regional climates. Indeed, CP-RCMs have been used to examine the possible effect of climate change on general thunderstorm activity (Rasmussen et al. 2020; Haberlie et al. 2022), MCSs (Prein et al. 2017, 2021; Haberlie and Ashley 2019b; Hwang et al. 2023; Dougherty et al. 2023), and even severe thunderstorms (Gensini and Mote 2014; Gensini and Mote 2015; Hoogewind et al. 2017; Molina et al. 2021; Ashley et al. 2023; Lasher-Trapp et al. 2023; Zeeb et al. 2024). Comparisons between CP-RCMs and GCMs have identified substantial differences in how societally relevant fields like precipitation totals

(Wallace et al. 2023) and severe weather frequency (Hoogewind et al. 2017) respond to climate change scenarios. The reported disparities between the two modeling approaches may be related by the complex relationship among changes in instability, convective inhibition, and thunderstorm initiation and sustenance in future climate change scenarios (Rasmussen et al. 2020; Haberlie et al. 2022; Ashley et al. 2023). These results suggest that regional responses to large-scale trends driven by global climate change can vary markedly and that the use of CP-RCMs is critical for improving our understanding in this area (Seneviratne et al. 2021; Prein et al. 2021; Kendon et al. 2021; Gensini 2021; Wallace et al. 2023). However, there is less confidence in the relationship between model performance gains and successively smaller CP-RCM grid spacings below 4 km. For example, Prein et al. (2021) and Wang et al. (2022) found that, although updraft intensity in simulated MCSs is underestimated at 4 km grid spacing, it is overestimated at sub-kilometer grid spacing. Thus, horizontal grid spacings near 4 km currently provide an acceptable balance of efficiency (i.e., processing time and data storage requirements) and effectiveness when simulating aspects of climate that are driven by mesoscale processes (Squitieri and Gallus 2022a, b; Ramos-Valle et al. 2023).

Recent work has leveraged CP-RCMs to examine the potential influence of climate change on MCS events in the CONUS (Prein et al. 2017, 2020; Haberlie and Ashley 2019b; Schumacher and Rasmussen 2020; Hwang et al. 2023; Dougherty et al. 2023). Initial work in this area has noted that MCSs in extreme climate change scenarios are larger in size and have increased maximum precipitation rates (Prein et al. 2017; Hwang et al. 2023; Dougherty et al. 2023). That said, existing studies have used a pseudo-global warming (e.g., Liu et al. 2017) approach with a single climate change scenario and invariant circulation features. In contrast, this work uses output from a CP-RCM that dynamically downscaled two climate change scenarios from a bias-corrected GCM (Gensini et al. 2023). As a result, both thermodynamic variables and circulation patterns may vary in response to climate forcing from the two scenarios. While circulation changes may be important for modeling changes in MCS activity (Harding and Synder 2015; Shaw et al. 2016; Feng et al. 2019; Song et al. 2021), this work focuses on connecting potential shifts in simulated MCS activity with reported changes in thermodynamic parameters and thunderstorm activity (Haberlie et al. 2022). Future work will focus on circulation features and their relationship to potential shifts in simulated MCS activity in climate change scenarios. While this "ensemble" approach of using two scenarios is still under dispersive and biased (Gensini et al. 2023), it provides a novel perspective of how organized deep, moist convection may respond to various climate change scenarios over the CONUS.

2 Data and methods

2.1 Convection-permitting regional climate model output

This work utilizes output from a suite of CP-RCM simulations (**WRF-BCC**; Gensini et al. 2023) that used the Weather Research and Forecasting Model (**WRF**) to dynamically downscale bias-corrected (Bruyère et al. 2014) Community Earth System Model (CESM; Hurrell et al. 2013) data. WRF-BCC has one retrospective experiment (1990–2005; **HIST**) and two end-of-21st-century (EoC; 2085–2100) experiments based on RCP 4.5 (**EoC 4.5**) and RCP 8.5 (**EoC 8.5**). Each experiment represents 15 continuously-integrated CP-RCM simulations from 45 water years (i.e., October–September).

Two variables from HIST, EoC 4.5, and EoC 8.5 are used in this work: 1) derived composite (vertical column maximum) reflectivity (REFD_COM) from the Thompson microphysics scheme (Thompson et al. 2008) to identify and track MCSs; and 2) total precipitation (AFWA_TOTPRECIP) from Air Force Weather Agency (AFWA) diagnostics (Creighton et al. 2014) to quantify precipitation associated with MCS events. Both variables have horizontal grid spacings of 3.75 km and 15-min temporal resolution. A full explanation of the WRF-BCC modeling approach and model verification can be found in Gensini et al. (2023). More details specific to this work can be found in Online Material 1 (Supplementary Description: Methods Supplement).

2.2 Identifying MCSs

MCSs are identified and tracked in 15-min derived composite reflectivity data from WRF-BCC (Gensini et al. 2023) to: 1) quantify MCS frequency; and 2) inform the process of identifying precipitation associated with MCSs (herein, MCS precipitation). MCSs are identified using a two-step process—segmentation (cf. Haberlie and Ashley 2018a) and tracking (cf. Haberlie and Ashley 2018b). Specific thresholds employed by this approach are based on the size, intensity, and duration proposed by Parker and Johnson (2000). Namely, MCSs are a system of deep, moist convective updrafts exceeding 100 km in one horizontal dimension that lasts for at least 3 h. These criteria are applied to sequences of 15-min derived composite reflectivity as described and demonstrated in previous work (Haberlie and Ashley 2018a, b, 2019a), including work using CP-RCM output from CONUS1 (Liu et al. 2017; Haberlie and Ashley 2019b) and WRF-BCC (Haberlie et al. 2023). More information on this approach can be found in Haberlie and Ashley (2018a, b) and in Online Resource 1 (Supplementary Description: Methods Supplement).

2.3 Derived statistics of MCSs

After tracking is completed, coordinates containing MCS tracks are used to make a 15-min MCS event mask, which is used to extract total precipitation (Figure S1 in Online Resource 1). MCS event and MCS precipitation data are resampled from 15-min to 1-h intervals, and spatial averaging is performed to aggregate the results from the 3.75 km WRF-BCC grid spacing to ~ 75-km analysis grids (i.e., 400 WRF-BCC grid cells per analysis grid), similar to the approach used in previous work (Hoogewind et al. 2017; Trapp et al. 2019; Haberlie et al. 2022; Haberlie et al. 2023). The analysis grids reduce the influence of spatial autocorrelation on the statistical tests and interpretation of the results, facilitate reasonable processing times, and retain much of the detail in the inherently smoothed seasonal and annual mean fields (Figure S2 in Online Resource 1). However, the spatial aggregation process removes extremes, so the analysis grids cannot be used to examine precipitation extremes associated with MCS events. Instead, annual and seasonal MCS day counts are calculated by determining how many "convective days" (i.e., 12 to 11 UTC; Hoogewind et al. 2017) experienced at least one hourly MCS event (i.e., the mean in the 75-km grid is greater than 0). This approach is sufficient for summarizing the initial annual and seasonal MCSs activity from WRF-BCC, while producing a smaller dataset that can be more easily acquired, compared, and replicated (Wilkinson et al. 2016).

2.4 Study region and definitions

The study region is constrained to states that are fully east of the Continental Divide (herein, ECONUS; Fig. 1.a) due to the relatively high rate of MCS events (Haberlie and Ashley 2019a; Cheeks et al. 2020; Feng et al. 2021). To compare regional responses to climate change scenarios, analysis grids within the ECONUS are further stratified by the subregions defined in Fig. 1.a—namely, Northern Plains (Fig. 1.a.i), Southern Plains (Fig. 1.a.ii), Midwest (Fig. 1.a.iii), Southeast (Fig. 1.a.iv), and Northeast (Fig. 1.a.v). To preserve space, regional statistics are denoted in the text using the 'reg' subscript (e.g., MCS_{reg}).

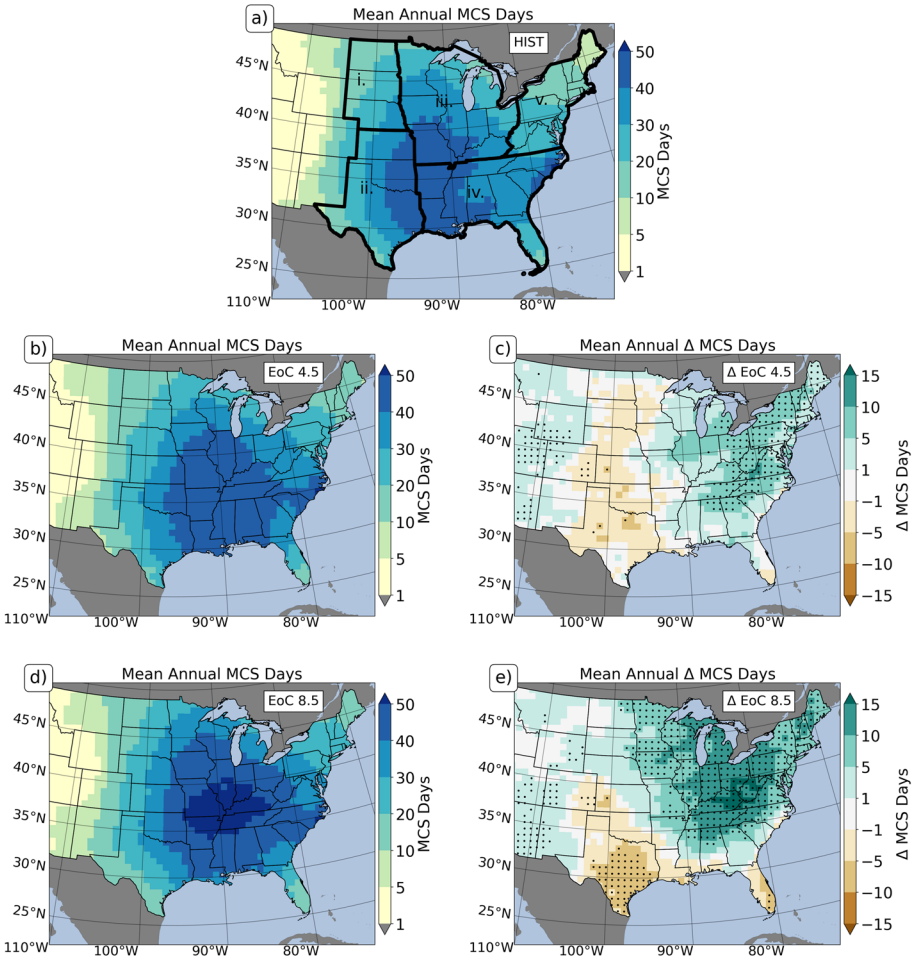

Fig. 1 MCS Mean annual MCS day counts for (**a**) HIST, (**b**) EoC 4.5, and (**d**) EoC 8.5, and changes in mean annual MCS day counts relative to HIST for (**c**) EoC 4.5 and (**e**) EoC 8.5. Analysis subregions in panel (a) include: (i) Northern Plains, (ii) Southern Plains, (iii) Midwest, (iv) Southeast, (v) Northeast, and (i-v) ECONUS. Stippling represents significant differences in mean annual MCS day counts between HIST and future scenarios (i.e., EoC 4.5 and EoC 8.5) based on the Mann–Whitney U test ($p < 0.05$) for that grid

2.5 Limitations

No attempt is made at quantitatively comparing observed and simulated MCS frequency and precipitation. In general, annual and seasonal precipitation totals and derived reflectivity events in HIST are comparable to observations (Haberlie et al. 2022; Gensini et al. 2023) and represent incremental improvements over similar CP-RCM experiments (e.g., Liu et al. 2017). Detections of MCS events are sensitive to observed and derived reflectivity thresholds (Haberlie and Ashley 2018a; Prein et al. 2023), and comparisons with observations can be heavily influenced by mismatched grid spacings, postprocessing assumptions, and noise and range-dependent issues (Smith et al. 1996). That said, derived reflectivity output from CP-RCMs has proven useful in studies focusing on climatic change (Trapp et al. 2019; Rasmussen et al. 2020; Haberlie et al. 2022). The results should be interpreted as differences between output from CP-RCM simulations representative of a "present" climate and two possible future climate change scenarios.

3 Results

3.1 MCS days in HIST

HIST produces patterns of annual and seasonal MCS activity that are comparable to existing research using the same tracking approach on observational data (Haberlie and Ashley 2019a). The patterns are generally similar to those reported by other observational studies of MCS activity (Cheeks et al. 2020; Feng et al. 2021), with some regional differences that may be owed to tracking decisions (Prein et al. 2023). Seasonal MCS activity in HIST (first column in Fig. 2) is similarly comparable to existing work (Feng et al. 2021)—namely, MCS activity is restricted to areas near the Gulf of Mexico in the winter, followed by a northern and western migration of events in the spring and summer, and, finally, a general reduction in frequency in the fall. Notably, the highest count of mean seasonal MCS days occurs in parts of Iowa and Minnesota during JJA (Fig. 2.g), producing spatial patterns and magnitudes comparable to observed MCS activity (Feng et al. 2021). These results provide confidence that the model can simulate MCSs as well as can be expected based on current modeling limitations and comparable CP-RCM results (Liu et al. 2017; Prein et al. 2020).

3.2 MCS days in EoC 4.5 and 8.5

3.2.1 Annual changes

Counts of annual MCS days vary significantly across the ECONUS (Fig. 1.b-e). In both EoC 4.5 (Fig. 1.b, c) and 8.5 (Fig. 1.d, e), MCS days generally decrease in the Southern Plains and increase in the Northeast. Although EoC 8.5 produces larger and more widespread differences, there are significant increases and decreases in both EoC 4.5 and 8.5. The largest significant increases in annual MCS days occur over parts of the Tennessee and Ohio River valleys in both EoC 4.5 and 8.5. The largest decreases occur in the Southern Plains in EoC 4.5 and 8.5, but few of the decreases in EoC 4.5 are significant.

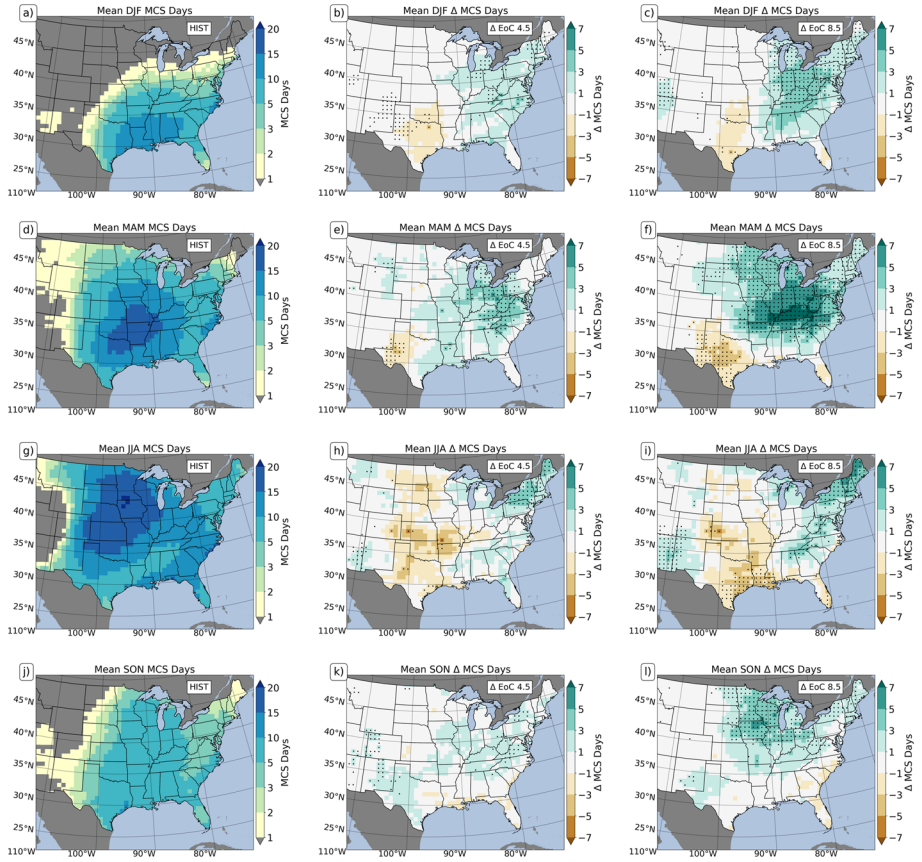

Fig. 2 As in Fig. 1, except for seasonal MCS days in (**a-c**) DJF, (**d-f**) MAM, (**g-i**) JJA, and (**j-l**) SON. Data in columns 2 and 3 are masked where HIST experiences fewer than 1 MCS day per year

The increases in annual MCS days are significant for almost every Northeast grid cell in both climate change scenarios.

Regional means of MCS day counts provide further context for the spatial trends in annual changes MCS activity (Fig. 3). Across the ECONUS, there is a general increase in annual MCS_{reg} days in both EoC 4.5 and 8.5, but these changes are only significant in EoC 8.5. Both the Midwest and Northeast experience significant increases in annual MCS_{reg} days in one or both climate change scenarios. In particular, the Northeast experiences significant increases in MCS_{reg} days for both EoC 4.5 and 8.5. Similarly, the Midwest experiences significant increases in MCS_{reg} days in EoC 8.5, but these increases are not significant in EoC 4.5. The other regions do not experience any significant changes in MCS_{reg} day counts. Comparing MCS_{reg} days between regions reveals a spatial shift in MCS activity in EoC 4.5 and 8.5. For example, the Southeast experiences more MCS_{reg} days per year than the Midwest in HIST, but fewer days per year on average in EoC 8.5. The Northeast experiences the largest increases in mean annual MCS_{reg} days in both EoC 4.5 and 8.5. In contrast, the Southern Plains experiences fewer MCS_{reg} days per year in EoC 4.5 and 8.5.

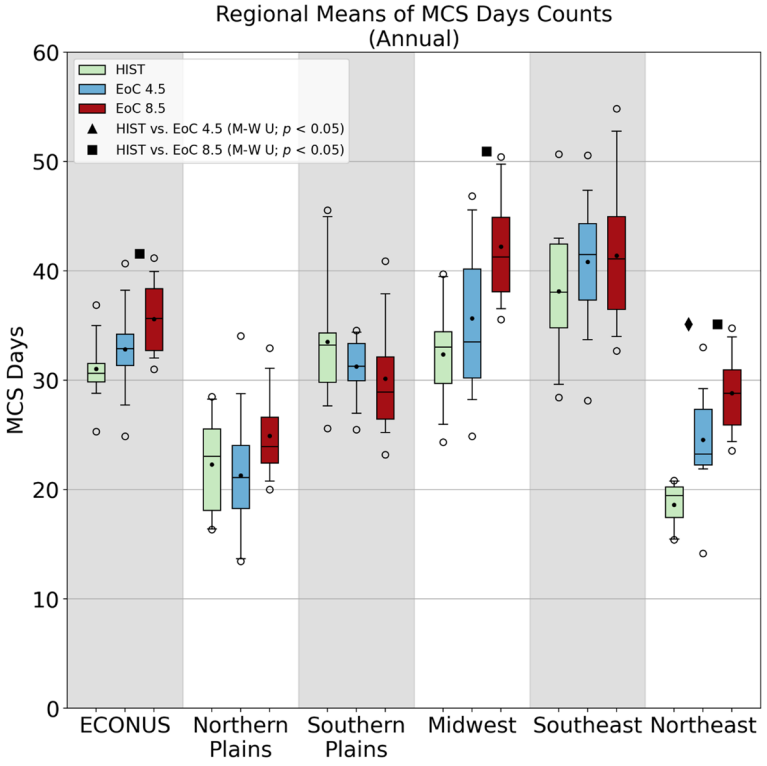

Fig. 3 Mean annual MCS days within the regions defined in Fig. 1.a. The boxplots illustrate the distribution of annual MCS days, and within each boxplot, the black dots denote the mean, the horizontal black lines represent the median, the box represents the interquartile range, the whiskers bound the 5th and 95th percentiles, the white circles represent outliers. The diamonds (squares) above the boxplots for each region represent significant differences between HIST and EoC 4.5 (EoC 8.5) based on the Mann–Whitney U test ($p < 0.05$)

3.2.2 Seasonal changes

The largest seasonal changes (Fig. 2; Figure S3 in Online Material 1) occur during MAM in the Ohio and Tennessee River valleys in EoC 8.5 (Fig. 2.f). This is juxtaposed with significant MAM decreases in mean annual MCS days in parts of the Southern Plains. In EoC 4.5, these changes are the result of a general northeastward shift in MAM MCS activity, with maximum ECONUS counts similar to those in HIST (Figure S3.d, e in Online Material 1). This northeastward shift is also present in EoC 8.5; however, MCS activity also increases in regions with relatively high HIST MCS day counts during MAM near the confluence of the Mississippi and Ohio rivers (Figure S3.f in Online Material 1). In contrast, fewer grid cells in the ECONUS experience significant changes in summertime MCS activity (Fig. 2.h, i). EoC 4.5 produces only sporadic significant changes in JJA MCS days, including some significant decreases in the Southern Plains. One notable regional exception is the Northeast, where both EoC 4.5 and 8.5 produce a spatially coherent cluster of significant increases in JJA MCS days. In both climate change simulations, there are no significant JJA changes within the main MCS corridor

in parts of the Midwest and Northern Plains. Spatial shifts in MCS activity during the winter are like those previously noted in the spring (Fig. 2.b, c), albeit with a more subtle northeastward expansion of MCS day counts in both EoC 4.5 and 8.5 that reach ECONUS maxima that are similar to HIST (Figure S3.b, c in Online Material 1). For SON, very few ECONUS grids experience significant changes in EoC 4.5 (Fig. 2.k), whereas EoC 8.5 produces a coherent cluster of significant increases in the Midwest (Fig. 2.l). Differences in the accumulation of annual MCS_{reg} days in the ECONUS (Fig. 4.a) are largely driven by MCS activity in both SON and MAM in EoC 8.5, and MAM in EoC 4.5 (Fig. 5). As a result, the distribution of annual accumulated MCS_{reg} days in EoC 8.5 diverges from those in HIST during the spring (Fig. 4.a). By March,

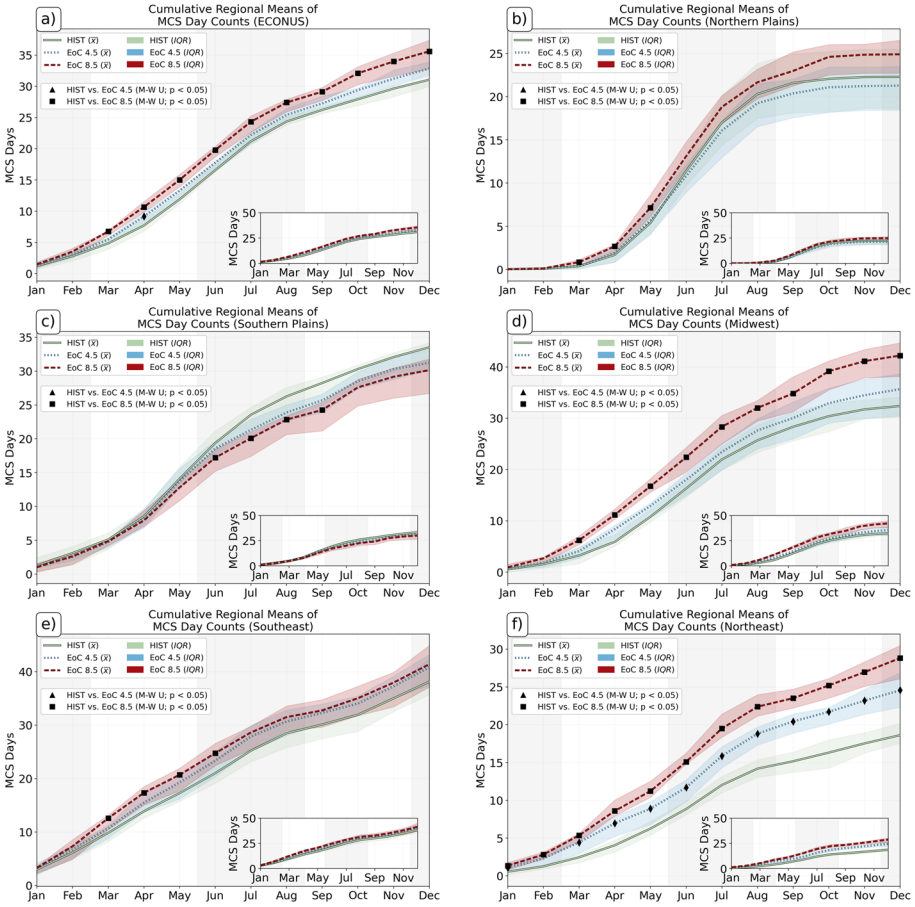

Fig. 4 Mean cumulative MCS days (lines) and interquartile ranges (shaded) for HIST (green), EoC 4.5 (blue), and EoC 8.5 (red). Mean MCS days within each region are accumulated monthly during each of the 15 simulation years. The analysis regions (Fig. 1.a) include (**a**) ECONUS, (**b**) Northern Plains, (**c**) Southern Plains, (**d**) Midwest, (**e**) Southeast, and (**f**) Northeast. The diamonds (squares) represent significant differences between HIST and EoC 4.5 (EoC 8.5) after the end of each simulation month during an annual period based on the Mann–Whitney U test ($p < 0.05$). The insets (bottom right) for each panel are the same data with a consistent y-axis range for all regions

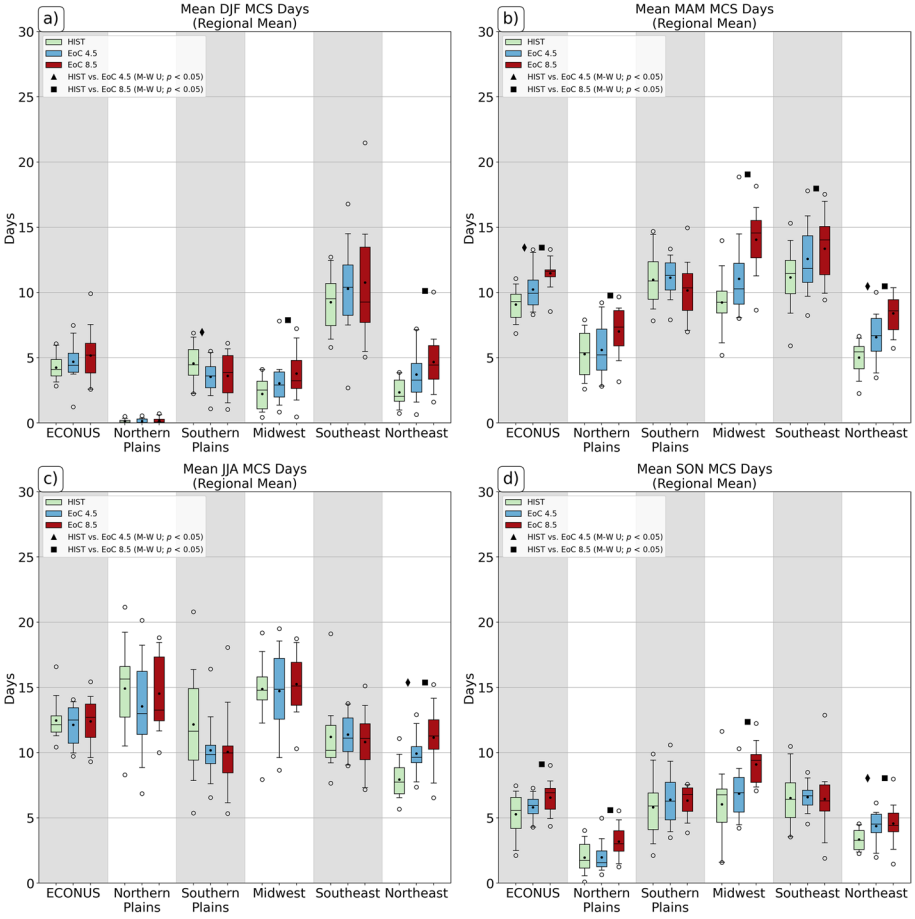

Fig. 5 As in Fig. 3, except for seasonal MCS days in (**a**) DJF, (**b**) MAM, (**c**) JJA, (**d**) SON

EoC 8.5 produces significantly more MCS_{reg} days than HIST across the ECONUS. In April, cumulative MCS_{reg} days significantly diverge from HIST for both EoC 4.5 and 8.5. Thereafter, the difference in cumulative MCS_{reg} days relative to HIST remains the same or slightly decreases through August in both climate change scenarios.

Subregional trends in cumulative and seasonal MCS_{reg} days exhibit some notable inter-regional variability. The strongest regional climate change signal occurs in the Northeast, where differences in cumulative annual MCS_{reg} days relative to HIST are significant for every month in EoC 8.5 and every month except February in EoC 4.5 (Fig. 4.f). These changes are driven by significant differences in MCS_{reg} day counts relative to HIST for every season in EoC 8.5, and every season except DJF in EoC 4.5 (Fig. 5). This region is also the only region to experience significant differences in JJA (Fig. 5.c). Similarly, the Midwest experiences significant departures from HIST in mean annual cumulative counts of MCS_{reg} days starting in March for EoC 8.5 (Fig. 4.d). Unlike the Northeast, however, the Midwest does not experience any significant seasonal differences in EoC 4.5, and summer MCS_{reg} day counts are comparable between HIST and the two climate change scenarios (Fig. 5.c). Both the Northern Plains (Fig. 4.b) and Southeast (Fig. 4.e) experience

significantly more cumulative MCS_{reg} days in EoC 8.5 by the end of May, but, like the Midwest, they experience no significant changes in MCS_{reg} day counts in JJA (Fig. 5.c). In contrast, the Southern Plains experience significantly fewer MCS_{reg} days by the end of August in EoC 8.5 compared to HIST (Fig. 4.c), but only experiences significant seasonal differences in DJF (Fig. 5.a).

3.3 MCS Precipitation in HIST

The patterns of annual and seasonal MCS precipitation in HIST (Fig. 6.a; first column Fig. 7) are consistent with MCS days (Fig. 1) and observed MCS precipitation (Haberlie and Ashley 2019a; Li et al. 2021). Like MCS days, MCS precipitation exhibits a strong and characteristic seasonal signal that is comparable with previous observational work (Li et al. 2021). The maximum mean seasonal MCS precipitation accumulation exceeds

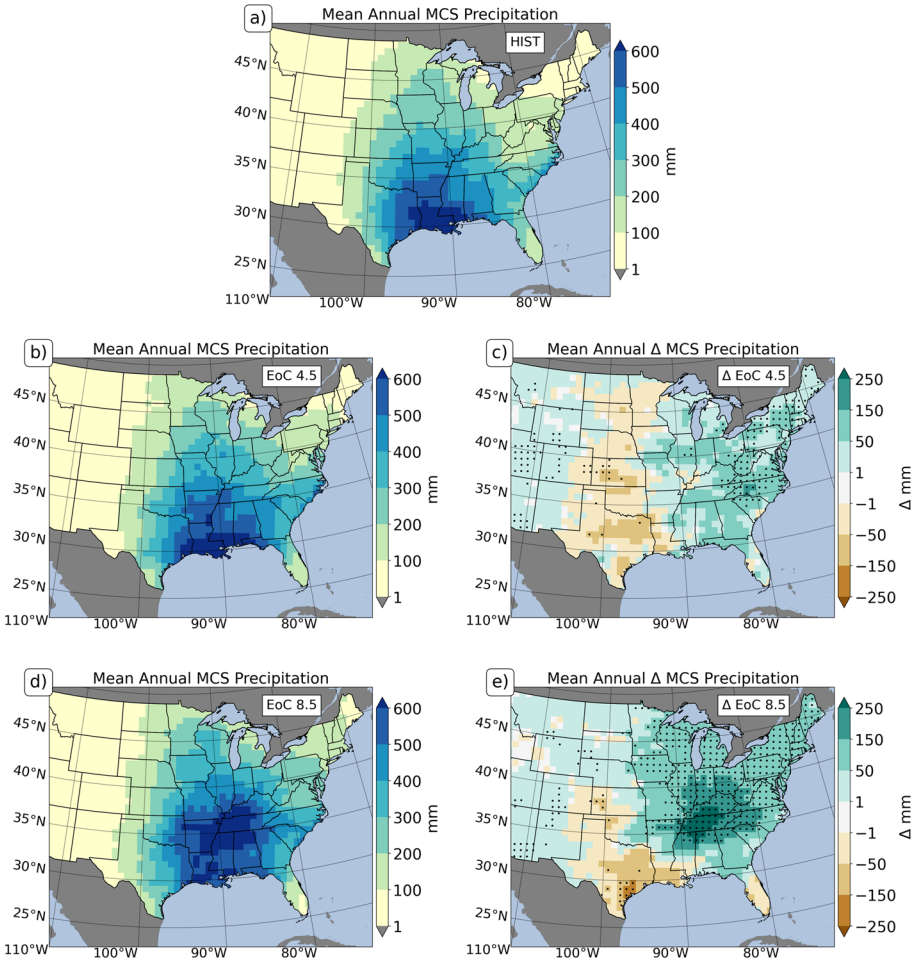

Fig. 6 As in Fig. 1, except for MCS precipitation and changes in MCS precipitation relative to HIST

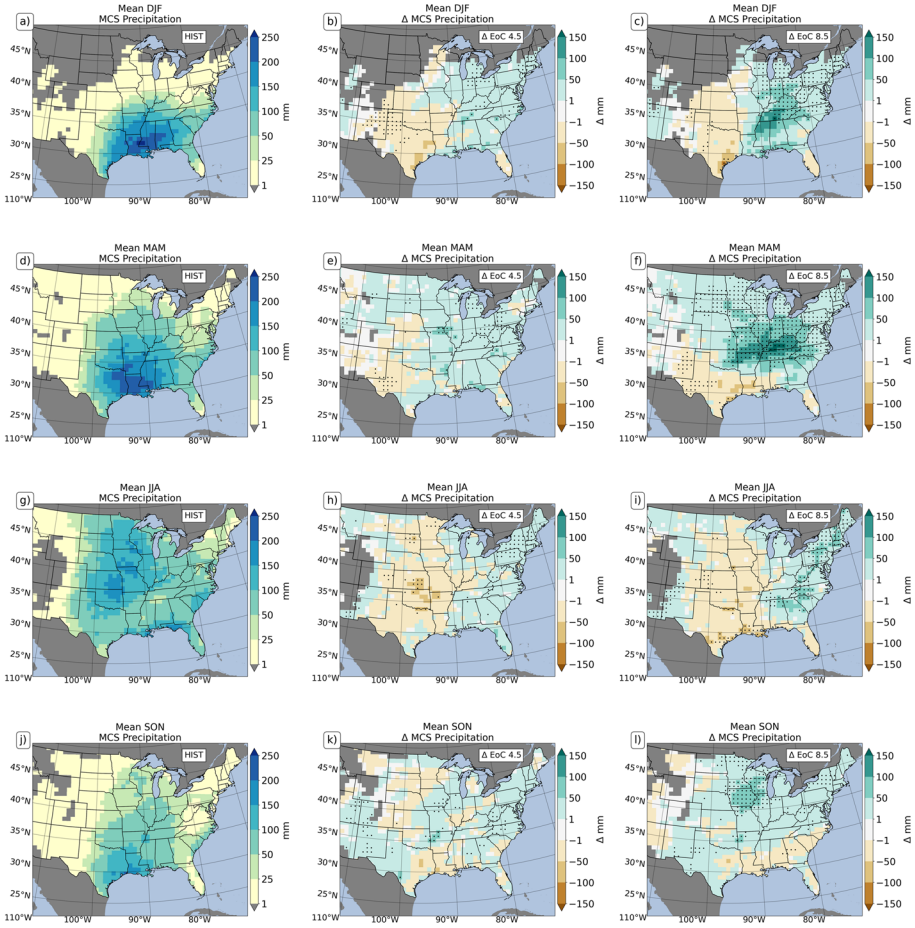

Fig. 7 As in Fig. 6, except for (**a-c**) DJF, (**d-f**) MAM, (**g-i**) JJA, (**j-l**) SON. Data in columns 2 and 3 are masked where HIST experienced less than 1 mm of mean seasonal MCS precipitation

250 mm season^{-1} in DJF (Fig. 7.a), whereas MAM experiences a maximum of 200 to 250 mm season^{-1} (Fig. 7.b), and JJA (Fig. 7.c) and SON (Fig. 7.d) have a maximum of 150 to 200 mm season^{-1}. Unlike the other seasons, the maximum JJA MCS precipitation values occur along an axis from Oklahoma to Wisconsin, which is consistent with observations (Haberlie and Ashley 2019a).

3.4 MCS Precipitation in EoC 4.5 and 8.5

3.4.1 Annual changes

Mean annual MCS precipitation exhibits marked variability across the ECONUS in the two climate change simulations (Fig. 6.b-e). As was the case with MCS days, MCS precipitation generally decreases in the Southern Plains and increases in the Northeast in

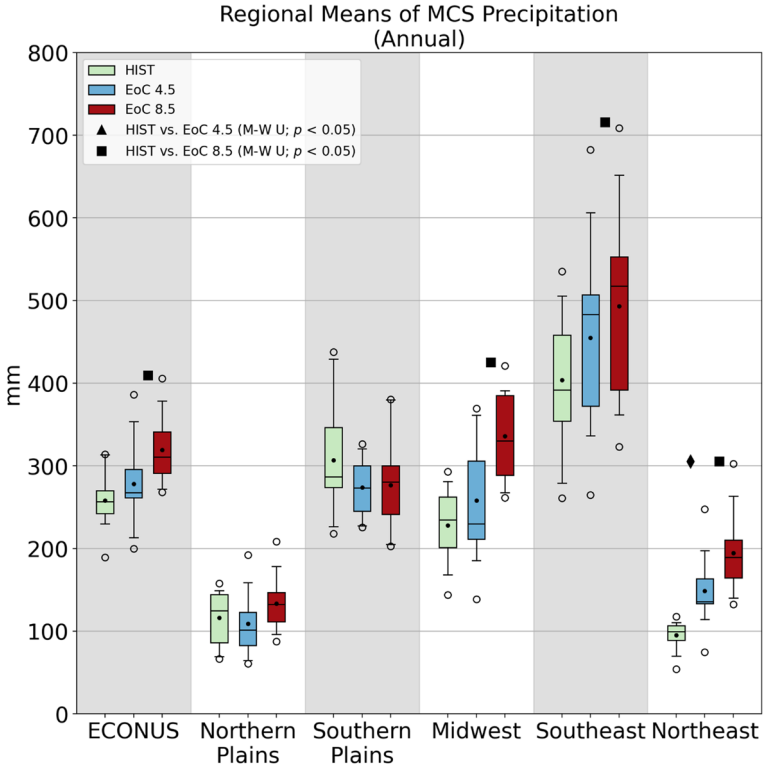

Fig. 8 As in Fig. 3, except for MCS precipitation

both EoC 4.5 and 8.5. Although significant ECONUS changes are more widespread in EoC 8.5, both EoC 4.5 and 8.5 produce significant increases in MCS precipitation in parts of the Northeast, as well as the Tennessee and Ohio River valleys. In contrast, parts of the Southern Plains experience MCS precipitation decreases in EoC 4.5 and 8.5. In general, both climate change simulations produce an eastward and northward expansion of higher MCS precipitation totals. For example, areas with the highest mean annual MCS precipitation totals are displaced hundreds of kilometers from the Gulf Coast in EoC 8.5 (e.g., ~ 35ºN latitude; Fig. 6.d), which is not the case in HIST (~ 30ºN latitude; Fig. 6.a).

Annual MCS_{reg} precipitation generally increases in all regions except the Northern and Southern Plains (Fig. 8). There is a general increase in annual ECONUS MCS_{reg} precipitation in both EoC 4.5 and 8.5, but these changes are only significant in EoC 8.5. Only the Northeast experiences significant increases in annual MCS_{reg} precipitation for both EoC 4.5 and 8.5. The Midwest and Southeast experience significant increases in annual MCS_{reg} precipitation only in EoC 8.5. This trend is also observed in the Southeast for both climate change scenarios. Although the changes are not significant, decreases in annual MCS_{reg} precipitation are experienced by both the Northern and Southern Plains in EoC 4.5, and just the Southern Plains in EoC 8.5.

3.4.2 Seasonal changes

Like MCS day changes, MAM experiences the largest seasonal changes in MCS precipitation (Fig. 7), specifically along an axis from eastern Oklahoma to eastern Kentucky (Fig. 7.f). The area of significant increases in MCS precipitation during MAM is expansive, and many of these grid cells experience 50% to over 100% increases in MCS precipitation in the pessimistic climate change scenario (Figure S5.f in Online Material 1). In EoC 4.5, however, there are far fewer grid cells that have significant increases in MCS precipitation during MAM (Fig. 7.e), though some grid cells experience 25% to over 100% more MCS precipitation relative to HIST (Figure S5.e in Online Material 1). DJF increases are also apparent in the same general areas in EoC 8.5 (Fig. 7.c). While EoC 8.5 amplifies mean DJF MCS precipitation totals in the lower Mississippi River valley, it produces a markedly different pattern during MAM compared to both HIST and EoC 4.5 (Figure S4.c, f in Online Material 1). This notable shift in maximum MCS precipitation totals may be related to changes in early warm-season circulation patterns (e.g., Song et al. 2018), and will be investigated in future work. Conversely, JJA precipitation decreases over most of the ECONUS (Fig. 7.h, i). Overall, the Northern and Southern Plains broadly exhibit 25% to 50% decreases in summertime MCS precipitation in both climate change scenarios, whereas the Midwest experiences both increases and decreases (Figure S5.h in Online Material 1). The Northeast is one exception to the general pattern of decreased MCS precipitation. In both EoC 4.5 and 8.5, the Northeast experiences anywhere from 10% to over 100% increases in JJA MCS precipitation. On an annual basis, the accumulation of MCS_{reg} precipitation in the ECONUS accelerates earlier in EoC 8.5 years, resulting in significant differences by March (Fig. 9.a). This difference remains relatively constant during the summer, and then increases in the fall. In contrast, EoC 4.5 produces smaller cumulative differences, and the mean remains in the interquartile for HIST throughout the year.

The variable subregional responses to the climate change scenarios are reflected in cumulative (Fig. 9) and seasonal (Fig. 10) MCS_{reg} precipitation. The Northeast experiences significant changes in cumulative MCS_{reg} precipitation in both EoC 4.5 and 8.5 (Fig. 10.f). By the end of May, cumulative MCS_{reg} precipitation increases by nearly 70% in EoC 4.5 and by over 140% in EoC 8.5 relative to HIST. By the end of the year, EoC 4.5 (8.5) experiences increases of 56% (105%) more MCS_{reg} precipitation compared to HIST. Additionally, this region experiences significant increases in seasonal MCS_{reg} precipitation (Fig. 10) in EoC 8.5 for all seasons. For EoC 4.5 in the Northeast, MAM, JJA, and SON experience significant increases in MCS_{reg} precipitation. There are no significant differences in cumulative or seasonal MCS_{reg} precipitation in EoC 4.5 for other regions. In EoC 8.5, the Northern Plains, Midwest, and Southeast experience differences in cumulative MCS_{reg} precipitation through parts of the year (Fig. 9.b, d, e), and during certain seasons (Fig. 10). Both the Midwest and the Southeast experience significant differences in cumulative MCS_{reg} precipitation by March in EoC 8.5, and finish the year with 47% and 22% more MCS_{reg} precipitation relative to HIST, respectively. Seasonally, the Midwest experiences significant increases in seasonal MCS_{reg} precipitation in DJF, MAM, and SON in EoC 8.5, whereas the Northern Plains only experiences significant increases in MAM. Notably, the Southeast does experience significant ($p < 0.05$) differences in the variability of MCS_{reg} precipitation in EoC 8.5 based on the Brown-Forsythe median test (Brown and Forsythe 1974). Southeast winters in the lower quartile for MCS_{reg} precipitation are similar in HIST and EoC 8.5, but upper quartile

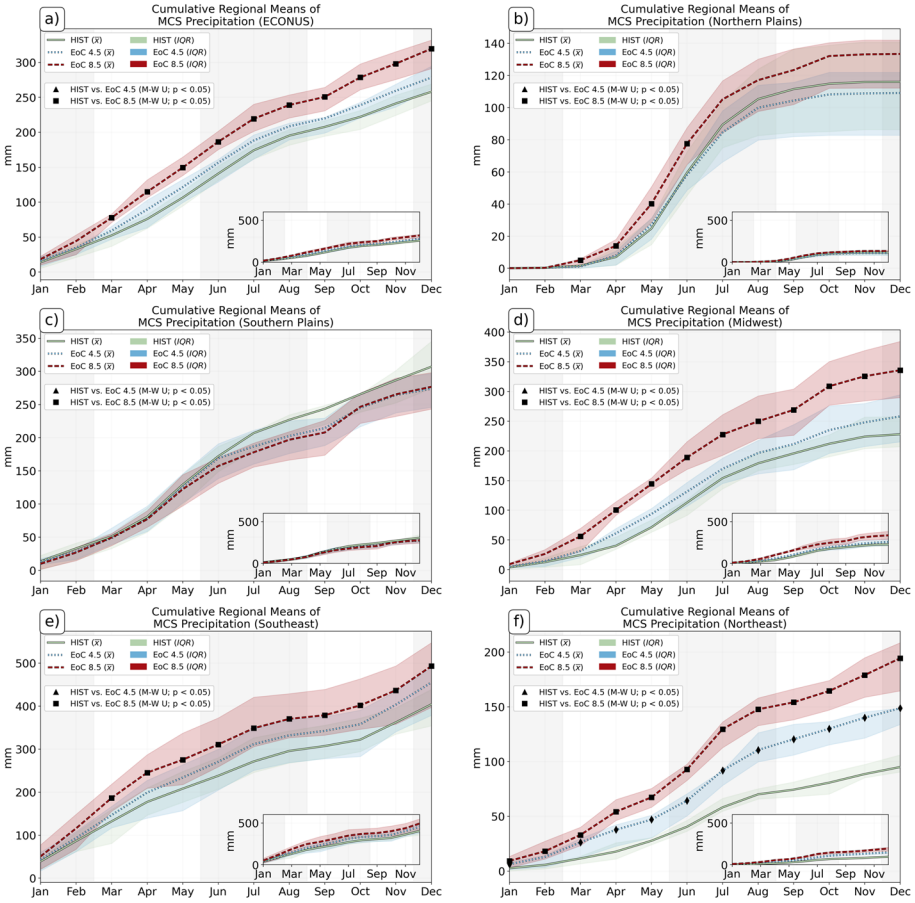

Fig. 9 As in Fig. 4, except for MCS precipitation

years in EoC 8.5 produce more precipitation than any DJF in HIST (Fig. 10). This significant variability may also explain why there is a lack of significant DJF differences in the southern Mississippi River Valley in EoC 8.5 (Fig. 7.c).

4 Possible drivers of change

4.1 Changes in MCS precipitation on MCS days

Changes in MCS precipitation may be driven by changes in frequency and/or intensity (Doswell et al. 1996). The results presented so far in this work suggest that MCS days and MCS precipitation exhibit changes (some significant) in both climate change scenarios. However, it is unclear if shifts in MCS precipitation are due to changes in the frequency of MCS days, or changes in MCS precipitation accumulation on MCS days. This is tested on a grid-by-grid cell basis by dividing MCS precipitation (Fig. 6) by MCS days (Fig. 1) and comparing those ratios in HIST to those in EoC 4.5 and 8.5 (Fig. 11). Any significant

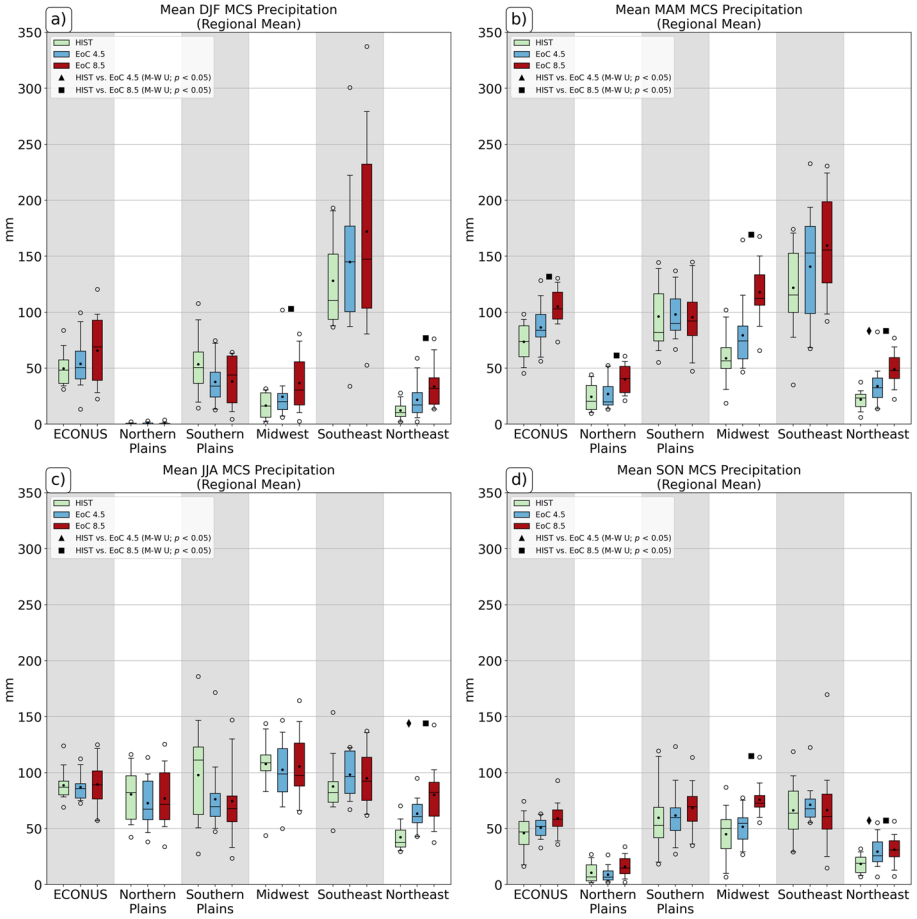

Fig. 10 As in Fig. 5, except for MCS precipitation

changes in this ratio could suggest that changes in either MCS days or MCS precipitation are a more important factor in the results reported in this work.

When an MCS day occurs near the Gulf Coast, MCS precipitation exceeds 13 mm day^{-1} in many locations in Louisiana, southern Mississippi, and eastern Texas (Fig. 11.a). These values remain relatively high throughout the Mississippi River Valley, with values exceeding 7 mm day^{-1} as far north as parts of Wisconsin. These values remain relatively similar in EoC 4.5 (Fig. 11.b), but a north and eastward expansion of higher values can be seen in EoC 8.5 (Fig. 11.d). Indeed, there are few significant changes in MCS precipitation on MCS days in EoC 4.5 (Fig. 11.c). In contrast, many grid cells in parts of the Ohio and Tennessee River valleys and Northeast experience significant increases in MCS precipitation on MCS days under EoC 8.5 that can exceed an average of 4 mm day^{-1} on an annual basis. EoC 8.5 also produces several clusters of significant seasonal changes in the ratio of MCS precipitation to MCS days, with some changes exceeding 5 mm day^{-1} (Figure S6 in Online Material 1). Conversely, EoC 4.5 experiences no widespread areas of significant changes in MCS precipitation to MCS day ratios.

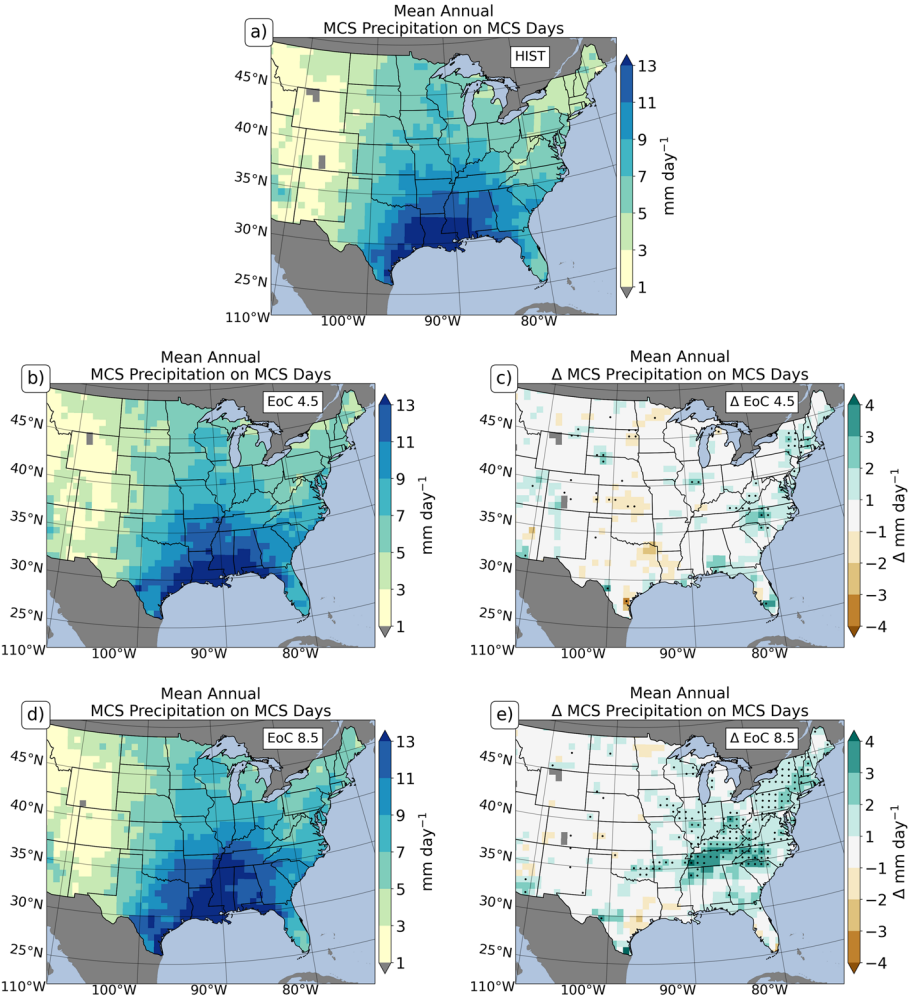

Fig. 11 As in Fig. 1, except for mean annual MCS precipitation on MCS days. Panels c and e are masked for grids where HIST has a value of less than 1 mm day.$^{-1}$

The ratio of MCS precipitation to MCS days significantly increases in EoC 8.5 over many of the same areas that experience the largest increases in MCS days (Fig. 1.d) and MCS precipitation (Fig. 6.d). One potential explanation is that MCSs have different characteristics (e.g., intensity, areal coverage, etc.) in EoC 8.5 compared to HIST that result in more precipitation on MCS days—this hypothesis will be tested in Section 4.2. From an environmental perspective, these changes may be due to shifts in pertinent thermodynamic environmental fields like CAPE and CIN (Hoogewind et al. 2017; Schumacher and Rasmussen 2020; Rasmussen et al. 2020; Haberlie et al. 2022; Ashley et al. 2023). WRF-BCC data have already been used to explore the relationship between thermodynamic changes (i.e., CAPE and CIN) and changes in thunderstorm activity across the ECONUS (Haberlie et al. 2022; Ashley et al. 2023). Those works found robust and widespread changes in CAPE across the ECONUS, whereas

the largest increases in CIN and decreases in thunderstorm activity occurred over the Great Plains. Generally, decreases in MCS activity are also collocated with the largest increases in CIN in EoC 4.5 and 8.5 (Haberlie et al. 2022). Conversely, increases in both MCS and thunderstorm activity over the Southeast, Midwest, and Northeast are associated with smaller increases in CIN and robust increases in CAPE. Increases in CAPE and days experiencing intense derived composite reflectivity values (e.g., ≥ 50 dBZ; Haberlie et al. 2022) in the same areas of robust increases in MCS precipitation on MCS days (Fig. 11.e) suggests that some MCS events are more intense in EoC 8.5 compared to HIST. Conversely, the more subtle changes in EoC 4.5 for both CAPE and CIN (Haberlie et al. 2022), and few differences in MCS precipitation on MCS days (Fig. 11.c), suggest that MCS events, in general, may not produce more precipitation than those in HIST. However, future work is needed to examine these issues in more detail, including how changes to pertinent circulation features modify MCS events in EoC 4.5 compared to 8.5.

4.2 Changes in MCS attributes

Relative to retrospective simulations, future climate change simulations have produced MCSs that are larger and more intense during their lifetimes (Prein et al. 2017; Dougherty et al. 2023), and existing observational analyses have also reported this trend (Feng et al. 2016). Thus, it follows that MCSs might also experience structural changes in EoC 4.5, 8.5, or both. Implicit evidence supporting this hypothesis was presented in Haberlie et al. (2022), who also found that the largest increases in "strong" thunderstorm activity in EoC 4.5 and 8.5 occurred in parts of the Midwest, Southeast, and Northeast. This hypothesis is explicitly tested by calculating various areal and intensity statistics based on derived composite reflectivity characteristics within the spatiotemporal bounds of qualifying MCS tracks (e.g., Figure S1 in Online Material 1). Specifically, the MCS lifetime maximum (i.e., the largest 15-min value from each MCS track) for the following attributes are examined: mean intensity, maximum intensity, and areal coverage of ≥ 20 dBZ, ≥ 40 dBZ, and ≥ 50 dBZ. Additionally, MCS track duration is included to examine if MCSs are lasting longer in EoC 4.5 or 8.5. These characteristics (Fig. 12) are comparable to those of observed MCSs reported in Haberlie and Ashley (2019a).

ECONUS MCSs exhibit significant changes in the mean annual values of every variable except duration in EoC 8.5 (Fig. 12). Additionally, both EoC 4.5 and 8.5 produce significant increases in mean annual maximum lifetime area covered by ≥ 50 dBZ, mean intensity, and maximum intensity. These results suggest that the changes depicted in MCS days and MCS precipitation in EoC 8.5 may be caused by MCS events that are larger and more intense, whereas EoC 4.5 trends are driven by increases in intensity. Notably, ECONUS changes in mean annual duration do not appear to be a contributing factor. These ECONUS trends are generally true for all seasons (Figure S7-10 in Online Material 1), with some exceptions. For SON, mean maximum lifetime area covered by ≥ 20 dBZ (Fig. 12.a) and mean maximum lifetime area covered by ≥ 40 dBZ (Fig. 12.b) decrease in EoC 4.5 and 8.5, with mean maximum lifetime area covered by ≥ 40 dBZ significantly decreasing in EoC 8.5. This change occurs despite significant increases in mean maximum lifetime area covered by ≥ 50 dBZ in both EoC 4.5 and 8.5. Only JJA experiences significant increases in mean maximum lifetime area covered

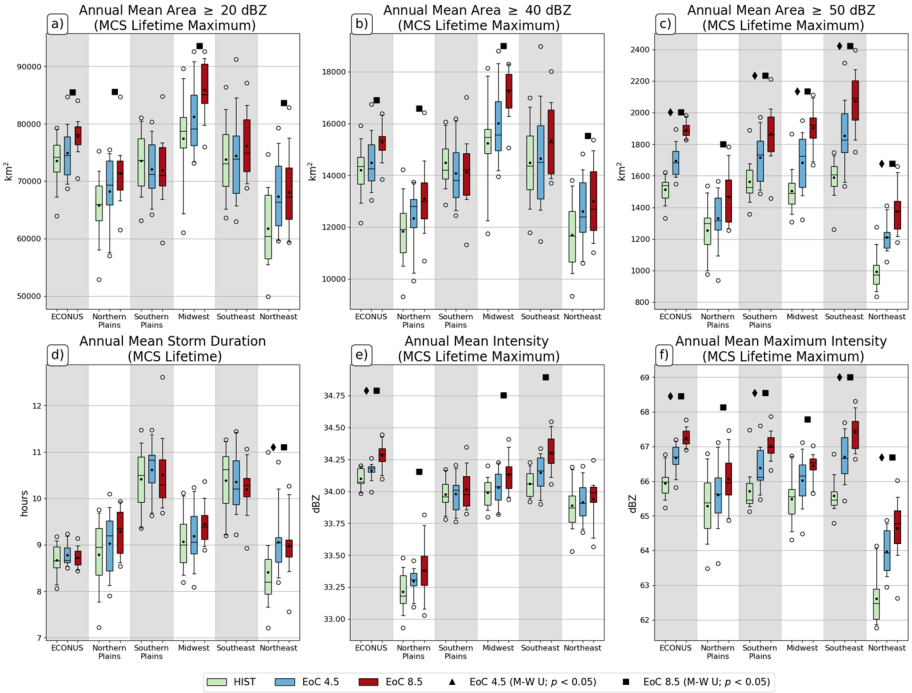

Fig. 12 As in Fig. 3, except for annual means of MCS lifetime maximum track attributes—namely (**a**) pixel area ≥ 20 dBZ, (**b**) pixel area ≥ 40 dBZ, (**c**) pixel area ≥ 50 dBZ, (**d**) track duration, (**e**) mean intensity (dBZ), and (**f**) maximum intensity (dBZ)

by ≥ 20 dBZ under EoC 8.5. These results suggest that while ECONUS MCSs in EoC 4.5 and 8.5 are not generally lasting longer, they are attaining a larger maximum areal extent, which agrees with previous work examining MCS trends (Feng et al. 2016) and simulated MCSs (Prein et al. 2017; Hwang et al. 2023). The increase in size is particularly true for the more intense derived composite reflectivity thresholds (i.e., 50 dBZ), which also agrees with previous work (Haberlie et al. 2022). Future work using WRF-BCC or other CP-RCM output should focus on 15-min or 1-h precipitation rates within MCS tracks to determine if there is a robust change in intensity throughout MCS lifecycles in EoC 4.5 and 8.5.

Regionally, the Southern Plains, Southeast, and Northeast all see significant increases in annual mean maximum lifetime area covered by ≥ 50 dBZ and maximum intensity under EoC 4.5 and 8.5 (Fig. 12). These trends remain in spring (Figure S8.c, f in Online Material 1) and summer (Figure S9.c, f in Online Material 1) for the Southeast and Northeast, but EoC 4.5 changes in mean maximum lifetime area covered by ≥ 50 dBZ and maximum intensity are not significant in the Southern Plains for MAM and JJA. In general, MAM and JJA produce the most significant differences, and some vary from annual differences. For example, the Midwest experiences significant increases in mean maximum lifetime area covered by ≥ 50 dBZ and maximum intensity in both EoC 4.5 and 8.5, whereas this was only the case for EoC 8.5 on an annual basis. Despite the lack of significant changes in MCS duration for the ECONUS, MCSs that traverse the Northeast have significantly longer durations in both EoC 4.5 and 8.5 (Fig. 12.d), despite

only experiencing significant increases in duration for EoC 8.5 in MAM (Figure S8.d in Online Material 1).

4.3 Changes in the diurnal cycle of MCSs during JJA

The development of MCSs requires sufficient moisture, instability, a source of lift, and vertical wind shear (Schumacher and Rasmussen 2020). The translation and maintenance of MCSs once they develop depends on these "ingredients" (Doswell et al. 1996) existing in the downstream environment, and supportive environments can be preconditioned hours or even days before the arrival of an MCS (Song et al. 2021). Despite the complexities, deep, moist convection generally follows a predictable diurnal pattern over the ECONUS during the warm season—namely, after initiating over the Great Plains (Weckwerth et al. 2004), individual storms interact and grow upscale to form MCSs (Coniglio et al. 2010) that propagate eastward (Carbone and Tuttle 2008). CP-RCM results have reported robust increases in CAPE across the ECONUS, but some areas like the Great Plains also experience comparatively large increases in CIN, with attendant decreases in thunderstorm activity (Rasmussen et al. 2020; Haberlie et al. 2022). Increased CIN may be causing the reduction in JJA MCS days (Fig. 2.h, i) and MCS precipitation (Fig. 7.h, i) by preventing convection initiation and/or upscale growth. This hypothesis is tested by examining seasonal differences in the diurnal cycle of JJA MCSs between HIST and EoC 4.5 and 8.5 (Fig. 13).

The observed diurnal cycle of JJA MCSs (Carbone and Tuttle 2008; Haberlie and Ashley 2019a; Cheeks et al. 2020; Li et al. 2021) is generally well-captured by HIST (first column in Fig. 13). HIST grid cell values for the late evening hours (Fig. 13.a) maximize in eastern Colorado, with a secondary maximum in Iowa. The High Plains maximum shifts east into western Kansas during the early morning (Fig. 13.d), and serves as the southwestern edge of an axis of increased MCS activity stretching northeastward into Minnesota. This region of elevated MCS activity shifts east and spans from eastern Oklahoma to western Wisconsin during the late morning (Fig. 13.g), and then widespread increases in MCS activity occur in the Midwest, Southeast, and Northeast during the afternoon (Fig. 13.j). The largest diurnal changes in JJA occur during the late evening in both EoC 4.5 and 8.5 (Fig. 13.b, c).

The critical MCS initiation area of eastern Colorado (Cheeks et al. 2020) experiences significant decreases in both climate change scenarios during the evening (00 – 05 UTC; Fig. 13.b, c). This region also experiences the largest increases in CIN (Haberlie et al. 2022), which may suppress the initiation and/or upscale growth of deep, moist convection. This overall reduction in activity likely manifests as reduced MCS days in downstream regions during the overnight hours (06 – 11 UTC; Fig. 13.e, f). However, there is a northward shift in the relative maximum of 06 – 11 UTC counts from southwestern Kansas in HIST to southeastern Nebraska in EoC 4.5 and 8.5 (Figure S11 in Online Material 1). While this results in only negligible increases in MCS activity for Nebraska, it may be the result of changes to the Great Plains low-level jet (Harding and Snyder 2015; Tang et al. 2017). Further, the Southern Plains experiences more widespread decreases in MCS days in EoC 4.5 (Fig. 13.b, e) compared to EoC 8.5, despite experiencing more subtle increases in CIN (Haberlie et al. 2022). Based on these results, future work should explicitly examine the influence of both thermodynamic and circulation features on the diurnal frequency of JJA MCSs.

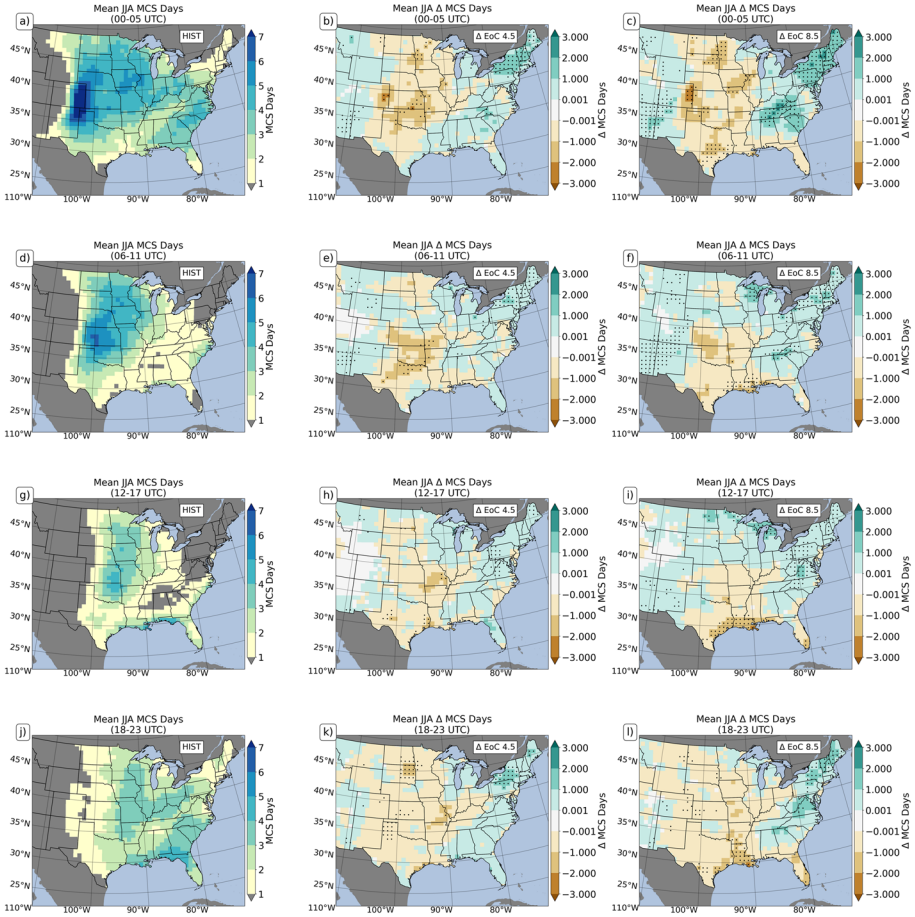

Fig. 13 As in Fig. 1, except for the mean count of JJA MCS days that experienced an MCS during a given hour (i.e., 0 – 23 UTC) averaged over 6-hourly periods—namely (**a-c**) 00 – 05 UTC, (**d-f**) 06 – 11 UTC, (**g-i**) 12 – 17 UTC, and (**j-l**) 18 – 23 UTC

5 Conclusions

The model output used for this work and described in Gensini et al. (2023) qualitatively captures the annual and seasonal patterns of observed MCS activity. The simulations based on RCP 4.5 (EoC 4.5) and RCP 8.5 (EoC 8.5) produce both significant increases and decreases in MCS activity and MCS precipitation across the ECONUS. While regions like the Southern Plains experience decreases in MCS activity in both EoC 4.5 and 8.5, the Midwest and Northeast experience increases in both MCS days and MCS precipitation. These results underscore the intricate regional disparities in MCS activity and precipitation projected in climate change scenarios, indicating considerable increases in both MCS days and MCS precipitation in certain areas like the Midwest, Southeast, and notably, the Northeast.

Contextualizing these results with prior research reveals that shifts in MCS activity align with observed (Rasmussen et al. 2023) and simulated (Haberlie et al. 2022;

Gensini et al. 2023; Haberlie et al. 2023) precipitation trends. When examining changes in MCS characteristics, the results suggest that MCSs are attaining larger maximum sizes and are more intense in EoC 4.5 and 8.5, which supports similar results reported in previous work (Feng et al. 2016; Prein et al. 2017; Hwang et al. 2023; Dougherty et al. 2023). Changes in MCS days, MCS precipitation, and MCS attributes are generally larger in EoC 8.5 compared to 4.5. The magnitude of changes in pertinent environmental parameters like CAPE and CIN in EoC 4.5 and 8.5 also mirrors this dichotomy (Haberlie et al. 2022; Ashley et al. 2023). More scenarios driven by CP-RCMs are needed to determine if there is a relationship between the magnitude of radiative forcing and changes in MCS attributes.

It is important to understand what physical processes and mechanisms are driving changes in MCS activity. Some of the changes are likely owed to how regional values of CAPE, CIN and precipitable water change in future climate scenarios (Haberlie et al. 2022; Prein et al. 2021; Hwang et al. 2023; Dougherty et al. 2023). However, very few studies have examined how future circulation shifts may influence MCS activity. Future work using CP-RCMs to examine potential changes in MCS activity under climate change scenarios should examine:

1) Potential shifts in the strength and location of the Great Plains low-level jet (Harding and Snyder 2015);
2) Changes in environmental variables that may influence the propagation and maintenance of MCSs (Corfidi 2003; Prein et al. 2020);
3) Trends in the location and intensity of mid-latitude cyclones and troughs (Shaw et al. 2016); and
4) Modification of the location and orientation of frontal boundaries, particularly during the summer, using automated frontal boundary detection tools (Justin et al. 2023).

CP-RCMs are necessary for realistically simulating mesoscale processes (Kendon et al. 2021; Prein et al. 2021). However, the strength of any conclusions based on CP-RCM output is currently limited by their immense computational, storage, and processing costs. For example, HIST, EoC 4.5, and EoC 8.5 required tens of millions of core hours to create using one of the most advanced computing clusters in the world. Despite this, the only differences between the three simulation groups are the initial and boundary conditions from CESM (Hurrell et al. 2013). Moving forward, our understanding of how climate change might influence mesoscale phenomena like MCSs could be improved by creating an ensemble of CP-RCMs that use different GCMs, greenhouse gas emission pathways, pseudo-global warming approaches, model configurations, modeling platforms, and time periods (Gneiting and Raferty 2005). Intradisciplinary and interdisciplinary cooperation will be required to efficiently use existing computational resources (Lagerquist et al. 2021; Schultz et al. 2021; Brotzge et al. 2023).

Supplementary Information The online version contains supplementary material available at https://doi.org/10.1007/s10584-024-03752-z.

Acknowledgements The authors would like to acknowledge high-performance computing support from Cheyenne (https://doi.org/10.5065/D6RX99HX) provided by NCAR's Computational and Information Systems Laboratory, sponsored by the National Science Foundation. The authors also would like to acknowledge and thank Dr. Michael Papka (Argonne) and the Argonne Leadership Computing Facility at Argonne National Laboratory for data storage and post processing assistance. This research used resources of the Argonne Leadership Computing Facility, which is a DOE Office of Science User Facility supported under Contract DE-AC02-06CH11357.

Funding This research was supported by the National Science Foundation award numbers 1637225, 1800582, and 2203516 and the National Oceanic and Atmospheric Administration award number NA22OAR4690645.

Data availability The code and dataset used for this study are available on GitHub (https://github.com/ahaberlie/MCS_Climate).

Declarations

Competing interests The authors have no relevant financial or non-financial interests to disclose.

References

Andrews M, Gensini VA, Haberlie A, Ashley WS, Taszarek M (2024) Climatology of the elevated mixed layer over the contiguous United States and northern Mexico using ERA5: 1979–2021. J Clim 37:1833–1851. https://doi.org/10.1175/JCLI-D-23-0517.1

Ashley WS, Haberlie AM, Strohm J (2019) A climatology of quasi-linear convective systems and their hazards in the United States. Weather Forecast 34:1605–1631

Ashley WS, Haberlie AM, Gensini VA (2023) The future of supercells in the United States. Bull Am Meteor Soc 104:E1-21. https://doi.org/10.1175/BAMS-D-22-0027.1

Brooks HE (2013) Severe thunderstorms and climate change. Atmos Res 123:129–138

Brotzge JA et al (2023) Challenges and opportunities in numerical weather prediction. Bullet Am Meteorol Soc 104:E698–E705

Brown MB, Forsythe AB (1974) Robust tests for the equality of variances. J Am Stat Assoc 69:364–367

Bruyère CL, Done JM, Holland GJ, Fredrick S (2014) Bias corrections of global models for regional climate simulations of high-impact weather. Clim Dyn 43:1847–1856

Carbone RE, Tuttle JD (2008) Rainfall occurrence in the US warm season: The diurnal cycle. J Clim 21:4132–4146

Cheeks SM, Fueglistaler S, Garner ST (2020) A satellite-based climatology of central and southeastern US mesoscale convective systems. Mon Weather Rev 148:2607–2621

Coniglio MC, Hwang JY, Stensrud DJ (2010) Environmental factors in the upscale growth and longevity of MCSs derived from Rapid Update Cycle analyses. Mon Weather Rev 138:3514–3539

Corfidi SF (2003) Cold pools and MCS propagation: Forecasting the motion of downwind-developing MCSs. Weather Forecast 18:997–1017

Creighton G, Kuchera E, Adams-Selin R, McCormick J, Rentschler S, Wickard B (2014) AFWA diagnostics in WRF. Fine Scale Models and Ensembles Team, 16th Weather Squadron, 2nd Weather Group, Air Force Weather Agency, University Corporation for Atmospheric Research, Northrop Grumman Corporation

Diffenbaugh NS, Scherer M, Trapp RJ (2013) Robust increases in severe thunderstorm environments in response to greenhouse forcing. Proc Natl Acad Sci 110:16361–16366

Doswell CA (1987) The distinction between large-scale and mesoscale contribution to severe convection: A case study example. Weather Forecast 2:3–16

Doswell CA, Brooks HE, Maddox RA (1996) Flash flood forecasting: An ingredients-based methodology. Weather Forecast 11:560–581

Dougherty EM, Prein AF, Gutmann ED, Newman AJ (2023) Future simulated changes in Central U.S, mesoscale convective system rainfall caused by changes in convective and stratiform structure. J Geophys Res: Atmos 128:e2022JD037537

Feng Z, Leung LR, Hagos S, Houze RA, Burleyson CD, Balaguru K (2016) More frequent intense and long-lived storms dominate the springtime trend in central US rainfall. Nat Commun 7:13429

Feng Z, Houze RA, Leung L, Song F, Hardin JC, Wang J, Gustafson WI, Homeyer CR (2019) Spatiotemporal Characteristics and Large-scale Environments of Mesoscale Convective Systems East of the Rocky Mountains. J Clim 32:7303–7328

Feng Z, Leung LR, Liu N, Wang J, Houze RA Jr, Li J, Hardin JC, Chen D, Guo J (2021) A global high-resolution mesoscale convective system database using satellite-derived cloud tops, surface precipitation, and tracking. J Geophys Res: Atmos 126:e2020JD034202

Gensini VA, Mote TL (2014) Estimations of hazardous convective weather in the United States using dynamical downscaling. J Climate 27:6581–6598. https://doi.org/10.1175/JCLI-D-13-00777.1

Gensini VA, Mote TL (2015) Downscaled estimates of late 21st century severe weather from CCSM3. Clim Change 129:307–321
Gensini VA, Haberlie AM, Ashley WS (2023) Convection-permitting simulations of historical and possible future climate over the contiguous United States. Clim Dyn 60:109–126
Gensini VA (2021) Severe convective storms in a changing climate. Climate change and extreme events (Ed) Fares A, Springer, 39–56. https://doi.org/10.1016/C2019-0-04922-9
Gneiting T, Raftery AE (2005) Weather forecasting with ensemble methods. Science 310:248–249
Haberlie AM, Ashley WS (2018a) A method for identifying midlatitude mesoscale convective systems in radar mosaics. Part I: Segmentation and classification. J Appl Meteorol Climatol 57:1575–1598
Haberlie AM, Ashley WS (2018b) A method for identifying midlatitude mesoscale convective systems in radar mosaics. Part II: Tracking. J Appl Meteorol Climatol 57:1599–1621
Haberlie AM, Ashley WS (2019a) A radar-based climatology of mesoscale convective systems in the United States. J Clim 32:1591–1606
Haberlie AM, Ashley WS (2019b) Climatological representation of mesoscale convective systems in a dynamically downscaled climate simulation. Int J Climatol 39:1144–1153
Haberlie AM, Ashley WS, Battisto CM, Gensini VA (2022) Thunderstorm activity under intermediate and extreme climate change scenarios. Geophys Res Lett 49:e2022GL098779
Haberlie AM, Ashley WS, Gensini VA, Michaelis A (2023) The ratio of mesoscale convective system precipitation to total precipitation increases in future climate change scenarios. Npj Clim Atmos Sci 6:150
Harding KJ, Snyder PK (2015) Using dynamical downscaling to examine mechanisms contributing to the intensification of Central US heavy rainfall events. J Geophys Res: Atmos 120:2754–2772
Hoogewind KA, Baldwin ME, Trapp RJ (2017) The impact of climate change on hazardous convective weather in the United States: Insight from high-resolution dynamical downscaling. J Clim 30:10081–10100
Houze RA (2018) 100 Years of research on mesoscale convective systems. Meteor Monogr 59:17.1-17.54
Hurrell JW et al (2013) The community earth system model: a framework for collaborative research. Bull Am Meteor Soc 94:1339–1360
Hwang Y, Zhao X, You C, Li Y (2023) Climatological features of future mesoscale convective systems in convection-permitting climate models using CMIP6 and ERA5 in the central United States.". Q J R Meteorol Soc 149:3135–3163
Justin AD, Willingham C, McGovern A, Allen JT (2023) Toward operational real-time identification of frontal boundaries using machine learning. Artif Intell Earth Syst 2:e220052
Kendon EJ, Prein AF, Senior CA, Stirling A (2021) Challenges and outlook for convection-permitting climate modelling. Phil Trans R Soc A 379:20190547
Lagerquist R, Turner D, Ebert-Uphoff I, Stewart J, Hagerty V (2021) Using deep learning to emulate and accelerate a radiative transfer model. J Atmos Oceanic Tech 38:1673–1696
Lasher-Trapp S, Orendorf SA, Trapp RJ (2023) Investigating a derecho in a future warmer climate. Bulletin of the American Meteorological Society. In Press
Lepore C, Abernathey R, Henderson N, Allen JT, Tippett MK (2021) Future global convective environments in CMIP6 models. Earth's Future 9:e2021EF002277
Li J, Feng Z, Qian Y, Leung LR (2021) A high-resolution unified observational data product of mesoscale convective systems and isolated deep convection in the United States for 2004–2017. Earth Syst Sci Data 13:827–856
Liu C et al (2017) Continental-scale convection-permitting modeling of the current and future climate of North America. Clim Dyn 49:71–95
Markowski P, Richardson Y (2011) Mesoscale meteorology in midlatitudes. Wiley
Molina MJ, Gagne DJ, Prein AF (2021) A benchmark to test generalization capabilities of deep learning methods to classify severe convective storms in a changing climate. Earth Space Sci 8:e2020EA001490
Nesbitt SW, Cifelli R, Rutledge SA (2006) Storm morphology and rainfall characteristics of TRMM precipitation features. Mon Weather Rev 134:2702–2721
Parker MD, Johnson RH (2000) Organizational modes of midlatitude mesoscale convective systems. Mon Weather Rev 128:3413–3436
Prein AF, Liu C, Ikeda K, Trier SB, Rasmussen RM, Holland GJ, Clark MP (2017) Increased rainfall volume from future convective storms in the US. Nat Clim Chang 7:880–884
Prein AF, Liu C, Ikeda K, Bullock R, Rasmussen RM, Holland GJ, Clark M (2020) Simulating North American mesoscale convective systems with a convection-permitting climate model. Clim Dyn 55:95–110

Prein AF, Rasmussen RM, Wang D, Giangrande SE (2021) Sensitivity of organized convective storms to model grid spacing in current and future climates. Phil Trans R Soc A 379:20190546
Prein AF et al (2023) Km-scale simulations of mesoscale convective systems (MCSs) over south america-a feature tracker intercomparison. Authorea Preprints. https://doi.org/10.22541/essoar.169841723.36785590/v1
Ramos-Valle AN, Prein AF, Ge M, Wang D, Giangrande SE (2023) Grid spacing sensitivities of simulated mid-latitude and tropical mesoscale convective systems in the convective gray zone. J Geophys Res: Atmos 128:e2022JD037043
Rasmussen KL, Prein AF, Rasmussen RM, Ikeda K, Liu C (2020) Changes in the convective population and thermodynamic environments in convection-permitting regional climate simulations over the United States. Clim Dyn 55:383–408
Rasmussen RM et al (2023) CONUS404: The NCAR-USGS 4-km long-term regional hydroclimate reanalysis over the CONUS. Bulletin of the American Meteorological Society. Accepted
Riemann-Campe K, Fraedrich K, Lunkeit F (2009) Global climatology of convective available potential energy (CAPE) and convective inhibition (CIN) in ERA-40 reanalysis. Atmos Res 93:534–545
Schultz MG, Betancourt C, Gong B, Kleinert F, Langguth M, Leufen LH, Mozaffari A, Stadtler S (2021) Can deep learning beat numerical weather prediction? Phil Trans R Soc A 379:20200097
Schumacher RS, Rasmussen KL (2020) The formation, character and changing nature of mesoscale convective systems. Nat Rev Earth Environ 1:300–314
Seneviratne SI et al (2021) Weather and climate extreme events in a changing climate. In: Climate Change 2021: The Physical Science Basis (Eds) Masson-Delmotte V et al, Cambridge University Press, 1513–1766
Shaw TA, Baldwin M, Barnes EA, Caballero R, Garfinkel CI, Hwang Y-T, Li C et al (2016) Storm track processes and the opposing influences of climate change. Nat Geosci 9(9):656–664
Smith JA, Seo DJ, Baeck ML, Hudlow MD (1996) An intercomparison study of NEXRAD precipitation estimates. Water Resour Res 32:2035–2045
Song F, Leung LR, Lu J, Dong L (2018) Future changes in seasonality of the North Pacific and North Atlantic subtropical highs. Geophys Res Lett 45:2018
Song F, Feng Z, Leung LR, Pokharel B, Wang S-YS, Chen X, Sakaguchi K, Wang C (2021) Crucial roles of eastward propagating environments in the summer MCS initiation over the US Great Plains. J Geophys Res: Atmos 126:e2021JD034991
Squitieri BJ, Gallus WA Jr (2022a) On the changes in convection-allowing WRF forecasts of MCS evolution due to decreases in model horizontal and vertical grid spacing. Part I: Changes in cold pool evolution. Weather Forecast 37:1903–1923
Squitieri BJ, Gallus WA Jr (2022b) On the changes in convection-allowing WRF forecasts of MCS evolution due to decreases in model horizontal and vertical grid spacing. Part II: Impacts on QPFs. Weather Forecast 37:1925–1940
Tang Y, Winkler J, Zhong S, Bian X, Doubler D, Yu L, Walters C (2017) Future changes in the climatology of the Great Plains low-level jet derived from fine resolution multi-model simulations. Sci Rep 7:5029
Taszarek M, Allen JT, Brooks HE, Pilguj N, Czernecki B (2021) Differing trends in United States and European severe thunderstorm environments in a warming climate. Bull Am Meteor Soc 102:E296–E322
Thompson G, Field PR, Rasmussen RM, Hall WD (2008) Explicit forecasts of winter precipitation using an improved bulk microphysics scheme. Part II: Implementation of a new snow parameterization. Mon Weather Rev 136:5095–5115
Trapp RJ, Hoogewind KA, Lasher-Trapp S (2019) Future changes in hail occurrence in the United States determined through convection-permitting dynamical downscaling. J Clim 32:5493–5509
Trenberth KE, Dai A, Rasmussen RM, Parsons DB (2003) The changing character of precipitation. Bull Am Meteor Soc 84:1205–1218
Wallace BC, Haberlie AM, Ashley WS, Gensini VA, Michaelis AC (2023) Decomposing the precipitation response to climate change in convection allowing simulations over the conterminous United States. Earth Space Sci 10:e2023EA003094
Wang D, Prein AF, Giangrande SE, Ramos-Valle A, Ge M, Jensen MP (2022) Convective updraft and downdraft characteristics of continental mesoscale convective systems in the model gray zone. J Geophys Res: Atmos 127:e2022JD036746
Weckwerth TM et al (2004) An overview of the International H2O Project (IHOP_2002) and some preliminary highlights. Bullet Am Meteorol Soc 85:253–278
Weisman ML, Skamarock WC, Klemp JB (1997) The resolution dependence of explicitly modeled convective systems. Mon Weather Rev 125:527–548

Wilkinson MD et al (2016) The FAIR Guiding Principles for scientific data management and stewardship. Sci Data 3:1–9
Zeeb AW, Ashley WS, Haberlie AM, Gensini VA, Michaelis AC (2024) Supercell precipitation contribution to the United States hydroclimate. Int J Climatol 44:1489–1512